Journal of
Materials Chemistry A

## Accepted Manuscript


This is an *Accepted Manuscript*, which has been through the RSC Publishing peer review process and has been accepted for publication.

*Accepted Manuscripts* are published online shortly after acceptance, which is prior to technical editing, formatting and proof reading. This free service from RSC Publishing allows authors to make their results available to the community, in citable form, before publication of the edited article. This *Accepted Manuscript* will be replaced by the edited and formatted *Advance Article* as soon as this is available.

To cite this manuscript please use its permanent Digital Object Identifier (DOI®), which is identical for all formats of publication.

More information about *Accepted Manuscripts* can be found in the **Information for Authors**.

Please note that technical editing may introduce minor changes to the text and/or graphics contained in the manuscript submitted by the author(s) which may alter content, and that the standard **Terms & Conditions** and the **ethical guidelines** that apply to the journal are still applicable. In no event shall the RSC be held responsible for any errors or omissions in these *Accepted Manuscript* manuscripts or any consequences arising from the use of any information contained in them.

Cite this: DOI: 10.1039/c0xx00000x

www.rsc.org/xxxxxx

ARTICLE TYPE

# Controlled synthesis of $TiO_2$ nanoparticles and nanospheres using microwave assisted approach with their application in dye-sensitized solar cells

**M. Ibrahim Dar,[a,b] Aravind Kumar Chandiran,[b] Michael Grätzel,*[b] Mohammad K. Nazeeruddin,*[b] and Srinivasrao A. Shivashankar*[a]**

***Received (in XXX, XXX) Xth XXXXXXXXX 20XX, Accepted Xth XXXXXXXXX 20XX***
**DOI: 10.1039/b000000x**

**Rapid and facile synthesis of ~7 nm and ~100-400 nm nanostructures of anatase titania is achieved by exploiting the chemical nature of solvents through the microwave based approach. After using these nanostructures as a photoanode in dye-sensitized solar cells, a modest yet appreciable efficiency of 6.5% was achieved under the illumination of one sun.**

Nanostructured transition metal oxides (TMO) are versatile materials with applications in various fields, such as photocatalysis,[1,2] magnetics,[3,4] energy storage,[5] and energy generation.[6,7] Among various TMO, $TiO_2$ (anatase) has been studied extensively in the context of dye-sensitized solar cells (DSC) and photo-assisted water-splitting.[1,7] As is well known, anatase is an n-type semiconductor with an indirect band gap of 3.2 eV. In the bulk, anatase is thermodynamically the least stable polymorph of $TiO_2$ but it has been shown that, in the nanometric regime (10-20 nm), anatase is the most stable polymorph.[8]

The confluence of electronic properties appropriate for energy harvesting,[9] with the stability,[10] renders anatase as the ideal photoanodic material in DSC. In fact, $TiO_2$ has been the inevitable anodic material since the first major breakthrough in the development of economical dye-sensitized solar cells was documented.[7] The biocompatibility or benign nature of $TiO_2$ also makes for its commercialization. Finally DSC technology has made its way towards large-scale application owing to several advantages, such as low-cost[7] and higher efficiency[11] which collectively make these energy generation devices more affordable.

Although various methods, such as sol-gel, reverse micelle, sonochemical, and solvothermal have been employed to synthesize $TiO_2$ nanostructures,[12-16] however, the best-performing mesoporous $TiO_2$ involves the hydrothermal method.[17] The conventional hydrothermal approach is really cumbersome and time-consuming. On the contrary, because of speed, homogeneous selective heating, and easy scalability, the solution-based, microwave-assisted approach to oxide synthesis has garnered much attention in recent years.[18] As such, the microwave-assisted method has been exploited for the synthesis of nanostructured $TiO_2$.[19] Chemical synthesis in the liquid phase through microwave irradiation involves heating that takes place majorly because of dipolar polarization and ionic conduction mechanisms.[18]

We report here a simple and novel approach to the microwave-assisted, solution-based synthesis of anatase $TiO_2$ nanostructures. Tuning of the morphology and size was achieved predictably by exploiting the nature of different solvents. Using such an approach, titania of different morphologies with the dimensions of ~7 nm and ~100-400 nm were synthesized, respectively, from the same thiobenzoate complex of titanium in benzyl alcohol and ethanol. After exposing the ethanolic and benzyl alcohol solutions to microwave irradiation for 10 and 30 minutes, respectively, the resulting powder samples were designated NS (ethanol) and NP (benzyl alcohol). The smaller (~7 nm) and the larger (~100-400 nm) $TiO_2$ nanostructures were used as the transparent and scattering layers, respectively, in dye-sensitized solar cells. To the best of authors' knowledge, there is no such report till date in the literature which brings out the synthesis of $TiO_2$ nanoparticles and nanospheres from a single precursor by employing such a facile approach and successfully exploited as anodic material in DSC.

Structural characterization of the resulting $TiO_2$ nanostructures was carried out using powder X-ray diffraction (XRD). The XRD patterns of as-prepared samples NP (Fig. 1a) and NS (Fig. 1b) are well defined and the patterns could be indexed to the tetragonal structure of $TiO_2$, JCPDS No. 21-1272. To within the detection limit of XRD, no peak characteristic of any impurity or of a different polymorph of $TiO_2$ was found in the samples. In addition the as-prepared nanostructures were crystalline, thus required no post-synthesis processing. The broad peaks are characteristic feature of the small crystallite size and applying the Scherrer equation to the most intense peak (101), the average crystallite sizes were determined to be 7 nm and 5 nm, respectively, for the NP and NS samples. The peaks in the XRD patterns are more intense in NP, which could be attributed to different nucleation and growth phenomena under dissimilar reaction conditions. As in contrast with NS, NP were obtained after 30 minutes of microwave irradiation of the solution in benzyl alcohol (see experimental section), which is also the solvent with the higher boiling point.

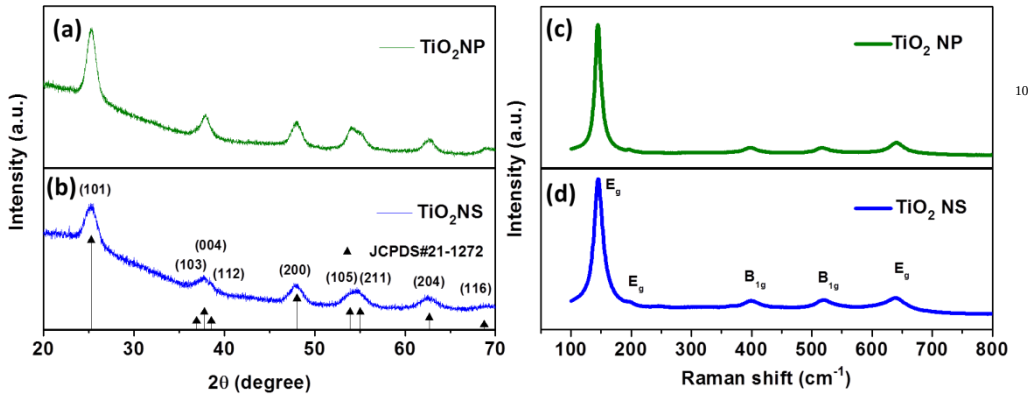


**Fig. 1** Powder XRD patterns (a, b) and room temperature Raman spectra (c, d) of $TiO_2$ (anatase) nanostructures.

Sensitivity of Raman spectral study to the presence of different polymorphs of titania was exploited to obtain further confirmation of the phase purity of the as-synthesized nanostructures of anatase $TiO_2$. The Raman spectra of the samples NP (Fig. 1c) and NS (Fig. 1d) show five peaks centered on 145 $cm^{-1}$, 199 $cm^{-1}$, 398 $cm^{-1}$, 518 $cm^{-1}$, and 639 $cm^{-1}$. The peaks at 145 $cm^{-1}$, 199 $cm^{-1}$and 639 $cm^{-1}$ could be assigned to the $E_g$ modes of vibration, whereas the peaks at 398 $cm^{-1}$and 518 $cm^{-1}$ could be assigned to the $B_{1g}$ modes of vibration.[20] The broadening and the systematic shifts in the frequencies of the various modes could be attributed to the small crystallite sizes.[21] No peak corresponding to any other polymorph of $TiO_2$ was observed in the Raman spectra.

The calculated crystallite size from the XRD peak broadening and the considerable FWHM of the most intense peak ($E_g$ = 145 $cm^{-1}$) in the Raman spectra clearly shows that the as-prepared NP and NS nanostructures comprise very fine anatase $TiO_2$ crystallites. The samples were therefore examined further by Transmission Electron Microscopy (TEM) (Fig. 2). The bright field TEM micrographs (BFTEM) of NP (Fig. 2e) display the presence of individual, acircular nanocrystals with an average diameter of ~ 6.5 nm. By contrast, the TEM micrographs of NS (Fig. 2a) show that the sample comprises nanospheres measuring 100–400 nm in diameter.

Such a size distribution shows apparent disagreement with the mean crystallite size deduced from the Scherrer equation, but the HRTEM (Fig. 2b) shows clearly that nanosphere is an aggregation of very small nanocrystals. The HRTEM of NS (Fig. 2b) and NP (Fig. 2f) display lattice fringes with *d* spacing of 3.5 Å, corresponding to the (101) plane of tetragonal (anatase) $TiO_2$, corroborating the FFT patterns shown in the inset. Furthermore, HRTEM also reveals that the size of nanocrystal is comparatively higher in NP (7 nm) compared to the crystallite size in NS (5 nm), in good agreement with the Scherrer equation. As already noted, the crystallites in NP are shape-anisotropic (elongated), whereas in the sample NS, the particles are more symmetrical (spherical). Selected area electron diffraction (SAED) from NS (Fig. 2c) and NP (Fig. 2g) shows ring patterns, confirming the polycrystalline nature of the samples; the patterns could be indexed to the tetragonal phase of $TiO_2$, thus corroborating XRD data. The particle size distribution, as deduced from histograms, reveals the high degree of mono-dispersity in NP (Fig. 2h), whereas an average diameter of ~295 nm can be assigned to the spherical entities in NS (Fig. 2d). It has to be noted that the particle size in NP refers to the extension along the axis and the histograms were constructed manually from the respective, depicted BFTEM micrographs.

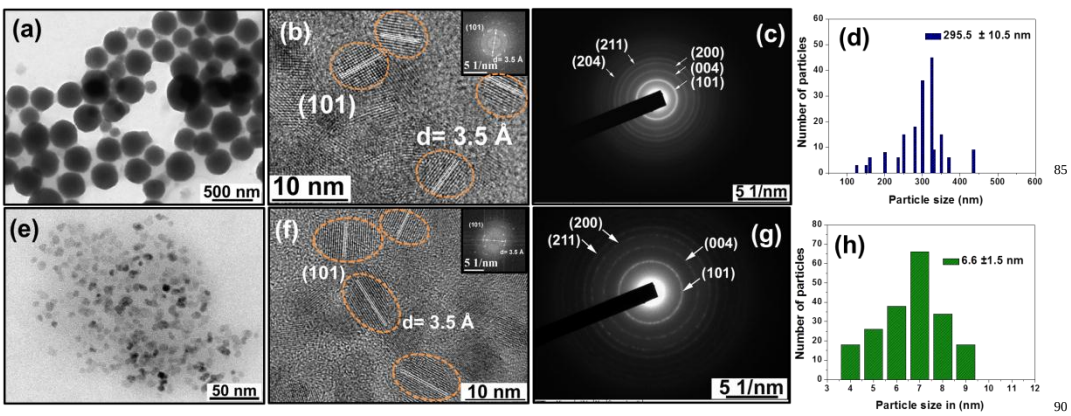


**Fig. 2** (a-d) Anatase nanospheres (sample NS), (e-h) Anatase nanoparticles (sample NP): (a), (e) BFTEM images, (b), (f) HRTEM images (inset: FFT patterns); (c), (g) SAED patterns corresponding to the tetragonal anatase phase and (d), (h) Histograms showing particle size distribution

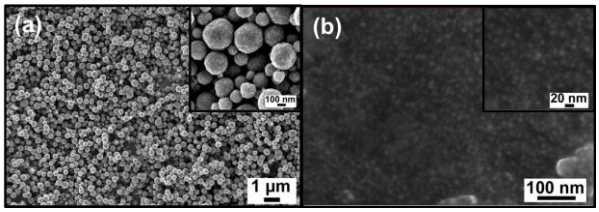


**Fig. 3** FESEM micrographs of anatase $TiO_2$ nanostructures; insets high magnification micrographs (a) Nanospheres (NS); (b) Nanoparticles (NP)

The samples NP and NS were examined for their gross morphology by field emission scanning electron microscopy (FESEM).The micrographs (Fig. 3a) reveal that very fine particles are packed densely into spherical aggregates, while the nanocrystals of NP (Fig. 3b) are rather fine, separated, and distinct. To understand the merits of microwave heating, we conducted the reaction in ethanol and benzyl alcohol under similar conditions, using conventional heating. FESEM analysis (Fig. S1) of the resulting samples shows the formation of aggregates without any defined morphology. Thus, we may infer that the conditions of reaction under microwave irradiation, such as the nature of the solvent, can lead to entirely different size and morphology of anatase $TiO_2$ nanostructures. A plausible mechanism for the formation of two distinct types of anatase nanostructures is proposed below.

It is to be noted that reaction in the medium of benzyl alcohol, a mildly coordinating solvent with a high boiling point resulted in the formation of monodisperse and well separated $TiO_2$ nanoparticles of the size ~7 nm. Benzyl alcohol is benign in nature,[22] and several reports have documented the non-aqueous synthesis of $TiO_2$ nanostructures, where benzyl alcohol has been employed as a solvent. Examples include the formation of crystalline nanoparticles *via* reaction between $TiCl_4$ and benzyl alcohol.[23] This contrasts with reaction in ethanol, a weak coordinating solvent with a higher loss tangent (0.941), which is also having lower boiling point, leading to the formation of nanospheres of the dimension of ~100-400 nm, in which nanocrystals of anatase are randomly oriented and densely packed.[19e] The impetus for such a randomly oriented aggregation could be the reduction of the overall energy resulting from the elimination of the surface energy associated with unsaturated bonding, i.e., the elimination of the solid-air or solid-liquid interfaces.[24] Given the rapidity with which the reaction occurs in the ethanolic medium, it is apparent that the aggregation observed is enabled by the rapid formation of nuclei and furthered by the absence of growth controlling or directing agent. Furthermore, the effect of nature of solvent could be traced by following the temperature profile of the reaction mixtures (Fig. S2). From the comparative analysis, the variation in the rate of heating is marginal, but could not be neglected. To examine the effect of duration of microwave exposure on the reaction pathway in benzyl alcohol, the reaction was terminated deliberately after 10 minutes; no precipitate formation was observed, unlike in ethanol, where the formation of $TiO_2$ nanospheres is complete within 10 minutes. The duration of microwave exposure was increased to 20 and 60 minutes, respectively, in ethanol and benzyl alcohol. TEM analysis (Fig. S3) shows that the increase in the dimensions of nanoparticles and nanospheres is negligible, indicating that the most of the precursor gets consumed within 10 and 30 minutes, respectively, in ethanol and benzyl alcohol. Similarly, when microwave power was reduced from 300 W to 150 W, no change in the morphology and dimensions was observed, as shown by BF-TEM micrographs (Fig. S4). However, when the concentration of the precursor was increased from 108mg/45 mL to 162 mg/45 mL in ethanol, a monotonic increase in the size of nanospheres is observed, as revealed by TEM analysis (Fig. S5). In addition to above reaction parameters, we also explored the impact of the solvent namely dimethylformamide (non-alcohol) on the morphology of the nanostructure. From the BF-TEM (Fig. S6), we observed the formation of dendrites comprised of fine nanostructures. We conclude that in addition to the other factors, the combination of the high loss tangent and the weak coordinating nature of ethanol leads to randomly oriented aggregation. The formation of well separated nanoparticles in benzyl alcohol may correspondingly be attributed to the slow rate of nucleation; also the solvent has comparatively a stronger coordinating nature. Furthermore, the dark field and bright field imaging obtained under Scanning Transmission Electron Microscope (STEM) mode for NS (Fig. 4 a, b) and NP (Fig. 4 e, f) samples corroborated the TEM and SEM data. Also the energy-dispersive X-ray spectroscopy under STEM mode (STEM-EDS) brought out the homogeneous distribution of Ti and O in the nanospheres (Fig. 3 c, d) and nanoparticles (Fig. 4 g, h).

X-ray photoelectron spectroscopy (XPS) was employed to carry out core level spectral analysis of titanium. The core shell XPS spectra (Fig. S7) reveal two strong peaks observed at 458.64 eV and 464.43 eV, which are in agreement with the binding energies of tetravalent Ti $2p_{3/2}$ and Ti $2p_{1/2}$, respectively.[25]

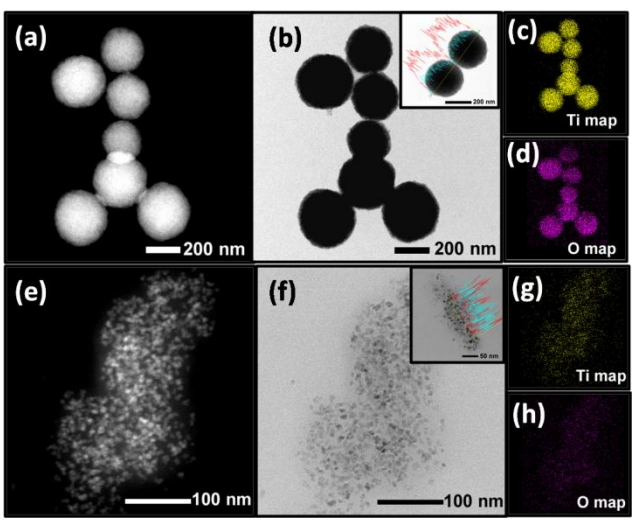


**Fig. 4** STEM of anatase $TiO_2$ nanostructures; (a,e) STEM dark field image, (b,f) STEM bright field image (inset: line scan mapping showing homogeneous presence of both elements (Ti & O)), Area maping (c,g) Ti map (d,h) O map

As no growth-controlling or precipitating agents were used in the synthesis, the resulting nanostructures were made of pure anatase, thus highly suitable for the solar cell applications. In a

conventional DSC, the transparent mesoporous layer is composed of $TiO_2$ nanoparticles of *ca*. 20 nm and the scattering layer contains bigger particles (~400 nm) to efficiently confine the unabsorbed higher wavelength photons within the photoanode film. As the morphology of the nanostructures could be controlled reliably using microwave synthesis, anatase $TiO_2$ of the two different sizes are used as transparent (NP) and scattering (NS) layers in DSCs. Samples NP and NS were made into a screen printing paste[26] and photoanode is printed (6 µm NP + 2 µm NS) on a conducting glass containing $TiCl_4$ underlayer. The complete photoanode preparation methods and the device fabrication techniques are reported in the supporting information. After sensitizing the photoanode with the ruthenium based C106 dye (Ru(4,4′-dicarboxylic acid-2,2′-bipyridine) (4,4′-bis(5-hexylthiophen-2-yl)-2,2′-bipyridine)$(NCS)_2$),[27] the devices were fabricated using our standard iodide/triiodide electrolyte (Z960) (for details see ESI) and platinum based counter electrode. The photovoltaic performances of the corresponding devices were analyzed under dark and AM 1.5G one sun irradiation (100 mW / $cm^2$) (Fig. 5a). Under illumination, the device exhibits a short-circuit current density ($J_{SC}$) of 12.6 $mAcm^{-2}$, an open-circuit voltage ($V_{OC}$) of 725 mV and a fill factor (FF) of 0.71, resulting in an overall conversion efficiency of 6.54 %. Fig. 5b shows the incident photon-to-current efficiency (IPCE), as a function of wavelength. The response of the present photovoltaic device to light could be related to short-circuit current and, at 550 nm, the IPCE reveals a maximum value of ~65 %.

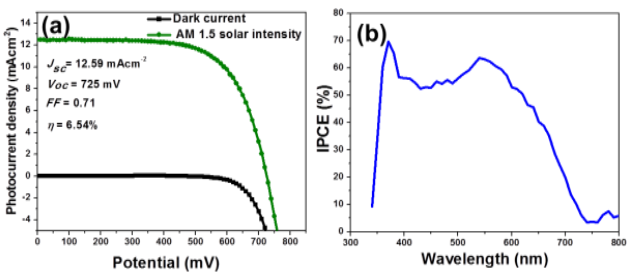


**Fig. 5** (a) Current-voltage (J-V) characteristics of devices under dark and irradiation at 100 $mWcm^{-2}$ photon flux (b) The IPCE spectrum as a function of the wavelength of monochromatic light for the device containing transparent (NP) and scattering (NS) layers.

To study the role of nanospheres (NS), a similar photoanode was printed (6 µm) containing only nanoparticles (NP). After sensitizing, the resulting device exhibits a short-circuit current density ($J_{SC}$) of 11.60 mA/$cm^2$, an open-circuit voltage ($V_{OC}$) of 732 mV and a fill factor (FF) of 0.68, resulting in an overall conversion efficiency (η) of 5.50% under illumination (100 mW / $cm^2$) (Fig. S8) and, at 550 nm, the IPCE (Fig. S8) with a maximum value of 55% was obtained.

The observed efficiencies are lower than those reported in the literature where state-of-the-art mesoporous $TiO_2$ films were sensitized with C106 dye.[27] The measured diminution in overall conversion efficiency in the present device is primarily due to the low JSC and this could be attributed to the two factors: (a) collapse of the transparent layers after sintering (from 12 µm as-printed to ~8 µm after sintering) due to the aggregation of small nanoparticles leading to the corresponding decrease in the surface area. The decrease in the surface area in turn affects the dye loading on the surface. (b) low transport rate of photogenerated electrons in the titanium oxide film comprising smaller particles. The smaller particles generally increase the electronic defect states both at interface and on the surface of the nanoparticles that in turn could affect the electron mobility within the film and hence the transport rate. Moreover, for a given recombination rate, the decline in the transport rate decreases the charge collection efficiency.[28]

## Conclusions

In summary, we have reported facile and novel synthesis of phase-pure anatase $TiO_2$ nanostructures through a microwave-assisted process in solution. Controlled synthesis of nanoparticles and nanospheres from the same precursor was achieved by exploiting the nature of the solvent. Detailed structural and morphological characterizations established the formation of phase-pure NP and NS. Furthermore, we show that such a methodology provides 'one-step' synthetic approach to make subsequently both the transparent (~7 nm) and scattering particles (~100-400 nm) for their application as a photoanode in dye-sensitized solar cells (DSC). Using standard Ru (II) polypyridyl sensitizer, a modest yet appreciable efficiency of 6.5% was achieved under the illumination of one sun (100 mW $cm^{-2}$ simulated AM 1.5 sunlight). We expect that the performance of the device can be further improved through the optimization of various parameters such as, increasing particle size of nanoparticles or changing the ratio of ethyl cellulose and titania. The efforts in this direction are under progress in our group.

## Experimental Section

Synthesis of $TiO_2$: In a typical synthesis, 108 mg of thiobenzoate complex of titanium, was dissolved in 45 ml of the solvent either ethanol or benzyl alcohol. The ethanolic and benzyl alcohol solutions were exposed to microwave irradiation for 10 and 30 minutes respectively, both leading to the formation of milky colloidal suspension.

**Table 1**: Summary of the experimental conditions used for the synthesis of various anatase $TiO_2$ nanostructures

| Solvent | Concentration (mg/mL) | Pressure (psi) | Power (W) | Time (minutes) | Temperature (°C) |
|---|---|---|---|---|---|
| Ethanol | 108 / 45 | 300 | 300 | 10 | 200 |
| Benzyl alcohol | 108 / 45 | 300 | 300 | 30 | 200 |
| Ethanol | 108 / 45 | 300 | 150 | 10 | 200 |
| Benzyl alcohol | 108 / 45 | 300 | 150 | 30 | 200 |
| Ethanol | 108 / 45 | 300 | 300 | 20 | 200 |
| Benzyl alcohol | 108 / 45 | 300 | 300 | 60 | 200 |
| Ethanol | 162 /45 | 300 | 300 | 10 | 200 |
| Dimethyl-formamide | 108 / 45 | 300 | 300 | 30 | 200 |

Brown powders were obtained from each suspension after centrifugation at 3000 rpm for 20 minutes. The powders were

washed twice with ethanol and dried at 60 °C under ambient conditions. The resulting powder samples were designated NS (ethanol) and NP (benzyl alcohol), respectively. The yield (> than 90%) obtained was somewhat higher when benzyl alcohol was used as the solvent. The conditions optimized for the synthesis of different anatase $TiO_2$ samples are summarized in Table 1.

## Acknowledgements

M.I.D gratefully acknowledges financial support from the Swiss confederation under Swiss Government Scholarship programme and UGC, India. M.I.D. and S.A.S thank to the Micro and Nano Characterization Facility, funded by NPMASS-DRDO and MCIT, Government of India. A.K.C, M.N.K and M.G acknowledge the financial contribution from European FP7 ORION project (NMP-229036).

## Notes and references

[a] *M. Ibrahim Dar, Prof. Srinivasrao A. Shivashankar, Centre for Nano Science and Engineering, Materials Research Centre, Indian Institute of Science, Bangalore 560012 India. Fax: (+)91 80 2360 4656 E-mail:shivu@cense.iisc.ernet.in*

[b] *M. Ibrahim Dar, Aravind Kumar Chandiran, Dr. Mohammad K. Nazeeruddin, Prof. Michael. Grätzel, Laboratory of Photonics and Interfaces, Institute of Chemical Sciences and Engineering, Swiss Federal Institute of Technology (EPFL), Station 6, 1015 Lausanne, Switzerland Fax: (+)41-216936100; E-mail:michael.graetzel@epfl.ch, mdkhaja.nazeeruddin@epfl.ch*

† Electronic Supplementary Information (ESI) available: [Materials, experimental section, characterization, device fabrication, temperature profiles, SEM, TEM and XPS data]. See DOI: 10.1039/b000000x/

1 A. Fujishima and K. Honda, *Nature* , 1972, **238**, 37.
2 A. Kubacka, M. Fernandez-García and G. Colon, *Chem. Rev.*, 2012, **112**, 1555.
3 A. H. Lu, E. L. Salabas and F. Schuth, *Angew. Chem. Int. Ed.*, 2007, **46**, 1222.
4 Z. Fang and K. Terakura, *J. Phys.: Condens. Matter*, 2002, **14**, 3001.
5 P. Poizot, S. Laruelle, S. Grugeon, L. Dupont and J. M. Tarascon, *Natur*e, 2000, **407**, 96.
6 A. Hagfeldt, G. Boschloo, L. Sun, L. Kloo and H. Pettersson, *Chem. Rev.*, 2010, **110**, 6595.
7 B. O'Regan and M. Graetzel, *Nature*, 1991, **353**, 737.
8 *(a)* U. Diebold, N. Ruzycki, G. S. Herman and A. Selloni, *Catal. Today*, 2003, **85,** 93; *(b)* A. S. Barnard and H. Xu, *ACS Nano*, 2008, **2,** 2237; *(c*) M. R. Ranade, A. Navrotsky, H. Z. Zhang, J. F. Banfield, S. H. Elder, A. Zaban, P. H. Borse, S. K. Kulkarni, G. S. Doran and H. J. Whitfield, *Proc. Natl. Acad. Sci. U.S.A.*, 2002, **99**, 6476.
9 *(a)* M. R. Hoffmann, B. T. Martin, W. Choi and D. W. Bahnemann, *Chem. Rev.*, 1995, **95**, 69; *(b*) M. Hincapie, M. I. Maldonado, I. Oller, W. Gernjak, J. A. Sanchez-Perez, M. M. Ballesteros and S. Malato, *Catal. Today*, 2005, **101**, 203.
10 H. K. Hashimoto, H. Irie and A. Fujishima, *Jpn. J. Appl. Phys*., 2005, **44**, 8269.
11 A. Yella, H. W. Lee, H. N. Tsao, C. Yi, A. K. Chandiran, M. K. Nazeeruddin, E. W. G. Diau, C. Y. Yeh, S. M. Zakeeruddin and M. Grätzel, *Science*, 2011, **334,** 629.
12 X. Chen and S. S. Mao, *Chem. Rev.*, 2007, **107**, 2891.
13 *(a)* T. Moritz, J. Reiss, K. Diesner, D. Su and A. Chemseddine, *J. Phys. Chem. B*, 1997, **101**, 8052; *(b)* D. M. Antonelli and J. Y. Ying, *Angew. Chem., Int. Ed*., 1995, **34**, 2014; *(c)* H. Zhang and J. F. Banfield, *J. Mater. Chem.*, 1998, **8**, 2073.
14 *(a*) J. Lin, Y. Lin, P. Liu, M. J. Meziani, L. F. Allard and Y. P. Sun, *J. Am. Chem. Soc*., 2002, **124**, 11514; *(b*) E. Stathatos, P. Lianos, F. Del Monte, D. Levy and D. Tsiourvas, *Langmui*r, 1997, **13**, 4295; *(c)* D. B. Zhang, L. M. Qi, J. M. Ma and H. M. Cheng, *J. Mater. Chem*., 2002, **12**, 3677;
15 *(a*) Y. C. Zhu, H. L. Li, Y. Koltypin, Y. R. Hacohen and A. Gedanken, *Chem. Commun.*, 2001, 2616; *(b)* J. C. Yu, J. G. Yu, W. K. Ho and L. Z. Zhang, *Chem. Commun.*, 2001,1942.
16 *(a*) R. R. Bacsa and M. Grätzel, *J. Am. Ceram. Soc*., 1996, **79**, 2185; *(b)* R. L. Penn and J. F. Banfield, *Geochim. Cosmochim. Acta*, 1999, **63**, 1549.
17 C. J. Barbe, F. Arendse, P. Comte, M. Jirousek, F. Lenzmann, V. Shklover and M. Grätzel , *J. Am. Ceram. Soc*., 1997, **80**, 3157.
18 I. Bilecka and M. Niederberger, *Nanoscale*, 2010, **2**, 1358.
19 *(a*) S Komarneni, R Roy and Q. H. Li, *Mater. Res. Bull.*, 1992, **27**, 1393; *(b*) S. Komarneni, R. K. Rajha and H. Katsuki, *Mater. Chem. Phys*., 1999, **61**, 50; *(c*) G. J. Wilson, G. D. Will, R. L. Frost and S. A. Montgomery, *J. Mater. Chem.*, 2002, **12**, 1787; *(d)* J. N. Hart, R. Cervini, Y. –B Cheng, G. P. Simon and L. Spiccia, *Solar Energy Mater. Solar Cells*, 2004, **84**, 135; *(e)* A. Jena, R. Vinu, S. A. Shivashankar and G. Madras, *Ind. Eng. Chem. Res*., 2010, **49**, 9636.
20 V. Swamy, A. Kuznetsov, L. S. Dubrovinsky, R. A. Caruso, D. G. Shchukin and B. C. Muddle, *Phys. Rev. B*, 2005, **71**, 184302/1.
21 X. Chen and S. S. Mao, *Chem. Rev.*, 2007, **107**, 2891.
22 N. Bindu, *Int. J. Toxicol.*, 2001, **20**, 23.
23 *(a)* M. Niederberger, M. H. Bartl and G. D. Stucky *J. Am. Chem. Soc*., 2002, **124**, 13642; *(b)* M. Niederberger, M. H. Bartl and G. D. Stucky, *Chem. Mater*., 2002, **14,** 4364.
24 *(a)* R. L. Penn and J. F. Banfield, *Science*, 1998, **281**, 969; *(b)* R. L. Penn, *J. Phys. Chem.* B, 2004, **108,** 12707; *(c)* M. I. Dar, S. Sampath and S. A. Shivashankar, *J. Mater. Chem*, .2012, **22**, 22418.
25 R. Sanjines, H. Tang, H. Berger, F. Gozzo, G. Margaritondo and F. Levy, *J. Appl. Phys*., 1994, **75**, 2945.
26 A. K. Chandiran, N. Tetreault, R. Humphry-Baker, F. Kessler, E. Baranoff, C. Yi, M. K. Nazeeruddin and M. Graetzel, *Nano Lett.*, 2012, **12,** 3941.
27 Y. Cao, Y. Bai, Q. Yu, Y. Cheng, S. Liu, D. Shi, F. Gao and P. Wang *J. Phys. Chem. C*, 2009, **113**, 6290.
28 L. M. Peter, *Phys. Chem. Chem. Phys.*, 2007, **9,** 2630.

**Table of content**

Here we report on 'one-step' synthetic approach to make both the transparent (~7 nm) and scattering particles (~100-400 nm) form a single precursor with their application as a photoanode in dye-sensitized solar cells (DSC).